

# Hamiltonian chaos and differential geometry of configuration space-time

Loris Di Cairano\*

*Institute of Neuroscience and Medicine INM-9, and Institute for Advanced  
Simulation IAS-5, Forschungszentrum Jülich, 52428 Jülich, Germany and  
Department of Physics, Faculty of Mathematics, Computer Science  
and Natural Sciences, Aachen University, 52062 Aachen, Germany*

Matteo Gori<sup>†</sup>

*Physics and Materials Science Research Unit, University  
of Luxembourg, L-1511 Luxembourg, Luxembourg*

Giulio Pettini<sup>‡</sup>

*Dipartimento di Fisica Università di Firenze, and I.N.F.N., Sezione  
di Firenze, via G. Sansone 1, I-50019 Sesto Fiorentino, Italy*

Marco Pettini<sup>§</sup>

*Aix-Marseille University, Marseille, France and  
CNRS Centre de Physique Théorique UMR7332, 13288 Marseille, France*

(Dated: January 28, 2022)

# Abstract

This paper tackles Hamiltonian chaos by means of elementary tools of Riemannian geometry. More precisely, a Hamiltonian flow is identified with a geodesic flow on configuration space-time endowed with a suitable metric due to Eisenhart. Until now, this framework has never been given attention to describe chaotic dynamics. A gap that is filled in the present work. In a Riemannian-geometric context, the stability/instability of the dynamics depends on the curvature properties of the ambient manifold and is investigated by means of the Jacobi–Levi-Civita (JLC) equation for geodesic spread. It is confirmed that the dominant mechanism at the ground of chaotic dynamics is parametric instability due to curvature variations along the geodesics. A comparison is reported of the outcomes of the JLC equation written also for the Jacobi metric on configuration space and for another metric due to Eisenhart on an extended configuration space-time. This has been applied to the Hénon-Heiles model, a two-degrees of freedom system. Then the study has been extended to the 1D classical Heisenberg  $XY$  model at a large number of degrees of freedom. Both the advantages and drawbacks of this geometrization of Hamiltonian dynamics are discussed. Finally, a quick hint is put forward concerning the possible extension of the differential-geometric investigation of chaos in generic dynamical systems, including dissipative ones, by resorting to Finsler manifolds.

PACS numbers: 05.20.Gg, 02.40.Vh, 05.20.- y, 05.70.- a

Keywords: Hamiltonian Chaos, Differential Geometry, Eisenhart metric

---

\* l.di.cairano@fz-juelich.de

† gori6matteo@gmail.com

‡ pettini@fi.unifi.it

§ pettini@cpt.univ-mrs.fr

## I. INTRODUCTION

As is well known, a rather common property of nonlinear dynamical systems, described by a system of differential equations, is the presence of *deterministic chaos* [1–3]. This means that despite the deterministic nature of a dynamical system of this kind, that is, despite the Cauchy’s theorem of existence and unicity of the solutions of differential equations, when describing a physical system by means of nonlinear differential equations the long time *predictability* of its behaviour is lost in the absence of *stability* of the dynamics. In other words, when we describe a physical system by means of a given dynamical system we are always making approximations, that is, we necessarily neglect all the remaining physical world. In so doing, even infinitesimal perturbations coming from all what has been neglected are necessarily amplified - destroying predictability - if a dynamical system is unstable with respect to variations of the initial conditions. Such a dramatic consequence of the breaking of integrability of a three body problem was already pointed out by Poincaré while describing the complexity of the homoclinic tangles in the proximity of hyperbolic points in phase space [4]. It was at the beginning of the 60’s of the last century that for the first time the consequences of homoclinic tangles in phase space of a nonlinear Hamiltonian system became visually evident. This was thanks to the numerical integration of the equations of motion of the celebrated Hénon-Heiles model [5]. The numerically worked out surfaces of section in phase space displayed what Poincaré declared to be unable even to dare to attempt drawing [6]. For many decades now, a huge amount of work has been done, both numerical and mathematical, on deterministic chaos. However, especially for many degrees of freedom systems, a theoretical explanation of the origin of chaos has been lacking. Homoclinic intersections certainly provide an elegant explanation of the origin of chaos in both dissipative and Hamiltonian systems. But this constructively applies - through Melnikov’s method - essentially to 1.5 or two degrees of freedom systems. Beautiful theorems on Axiom A systems [1] and Anosov flows [7] cannot account for the emergence of chaos in dynamical systems of physical relevance. An independent attempt to explain the origin of chaos in Hamiltonian systems was put forward by N.S.Krylov who resorted to the possibility of identifying a Hamiltonian flow with a geodesic flow in configuration space to try to explain the origin of the dynamical instability (which we nowadays call deterministic chaos) that could explain the spontaneous tendency to thermalization of many body systems. Krylov’s

pioneering approach focused on the search for negative curvatures in configuration space equipped with a suitable metric [8]. Krylov's work inspired abstract ergodic theory but did not go too far to explain the origin of chaos in Hamiltonian dynamical systems. For instance, in the case of the already mentioned Hénon-Heiles model, it turns out that no region of negative curvature can be found in configuration space, therefore Krylov's intuition has been discarded for a long time. However, more recently, on the basis of numerical "experiments" it has been shown that chaos in Hamiltonian flows of physical relevance stems from another mechanism, parametric instability, which will be discussed throughout this paper. The Riemannian-geometric approach to explaining the origin of chaos in Hamiltonian flows is based on two fundamental elements [10]: *i*) the identification of a Hamiltonian flow with a geodesic flow of a Riemannian manifold equipped with a suitable metric, so that the geodesic equations

$$\frac{d^2 q^i}{ds^2} + \Gamma_{jk}^i \frac{dq^j}{ds} \frac{dq^k}{ds} = 0 . \quad (1)$$

coincide with Newton's equations

$$\frac{d^2 q^i}{dt^2} = - \frac{\partial V(q)}{\partial q^i} . \quad (2)$$

a Hamiltonian flow - of which the kinetic energy is a quadratic form in the velocities, that is,  $H = \frac{1}{2} a_{ik} p^i p^k + V(q_1, \dots, q_N)$  - is equivalent to the solutions of Newton's equations of motion stemming from a Lagrangian function  $L = \frac{1}{2} a_{ik} \dot{q}^i \dot{q}^k - V(q_1, \dots, q_N)$ ;

*ii*) the description of the stability/instability of the dynamics by means of the Jacobi-Levi-Civita (JLC) equation for the geodesic spread measured by the geodesic deviation vector field  $J$  (which locally measures the distance between nearby geodesics), which in a parallel-transported frame reads

$$\frac{d^2 J^k}{ds^2} + R_{ijr}^k \frac{dq^i}{ds} J^j \frac{dq^r}{ds} = 0 . \quad (3)$$

where  $R_{ijr}^k$  are the components of the Riemann-Christoffel curvature tensor.

The most natural geometrization of Hamiltonian dynamics in a Riemannian framework [9] is a consequence of Maupertuis least action principle for isoenergetic paths

$$\delta \int_{q(t_0)}^{q(t_1)} dt W(q, \dot{q}) = 0 , \quad (4)$$

where  $W(q, \dot{q}) = \{[E - V(q)] a_{ik} \dot{q}^i \dot{q}^k\}^{1/2}$ , which is equivalent to the variational definition of a *geodesic* line on a Riemannian manifold, a line of stationary or minimum length joining



the points  $A$  and  $B$ :

$$\delta \int_A^B ds = 0 . \quad (5)$$

If the subset of configuration space  $M_E = \{(q_1, \dots, q_N) \in \mathbb{R}^N | V(q_1, \dots, q_N) < E\}$  is given the non-Euclidean metric  $g_J$  of components

$$(g_J)_{ij} = 2[E - V(q)]a_{ij} , \quad (6)$$

whence the infinitesimal arc element  $ds^2 = 4[E - V(q)]^2 dq_i dq^i$ , then Newton's equations (2) are retrieved from the geodesic equations (1) of the manifold  $(M_E, g_J)$ .

The JLC equation for the geodesic spread can be rewritten as [11]

$$\frac{d^2 J^k}{ds^2} + 2\Gamma_{ij}^k \frac{dq^i}{ds} \frac{dJ^j}{ds} + \left( \frac{\partial \Gamma_{ri}^k}{\partial q^j} \right) \frac{dq^r}{ds} \frac{dq^i}{ds} J^j = 0 , \quad (7)$$

which has general validity *independently* of the metric of the ambient manifold.

Importantly, there are other Riemannian manifolds, endowed with different metric tensors, to geometrize Hamiltonian dynamics [11]. Two of these alternatives are concisely described in the following. One brings about the standard tangent dynamics equation as geodesic spread (JLC) equation, whereas the second one has never been investigated hitherto to describe chaos in Hamiltonian flows. This gap is filled in the present work. The choice among these manifolds is driven by practical computational reasons as will be discussed in what follows.

## II. WHY A RIEMANNIAN APPROACH TO HAMILTONIAN CHAOS

There are several phenomenological descriptions of chaos in nonlinear dynamical systems. For two-degrees of freedom Hamiltonian flows, Poincaré surfaces of section are very effective. At arbitrary number of degrees of freedom, for instance, the development of a continuous component in the frequency spectra of the variables of the system is a typical consequence of a chaotic dynamics. However, the paradigmatic phenomenological indicator, and quantitative measure, of chaotic behaviour of a flow is the largest Lyapunov exponent  $\lambda_1$ , but detecting chaos does not explain its cause. Let us concisely summarize a physicist's point of view on what motivates resorting to the Riemannian approach. As mentioned in the Introduction, the classical explanation of the origin of chaos is based on homoclinic tangles discovered by Poincaré and culminated in the Smale-Birkhoff homoclinic theorem. This

theorem states that if a diffeomorphism  $\varphi : M \rightarrow M$  of an  $n$ -dimensional manifold  $M$  has a hyperbolic fixed point  $\tilde{x}$  with associated stable  $W^s(\tilde{x})$  and unstable  $W^u(\tilde{x})$  manifolds that intersect transversely at some point  $x_0 \neq \tilde{x}$  then a hyperbolic invariant set  $\Lambda \subset M$  exists which is invariant under the action of  $\varphi$ . A conceptually powerful theorem indeed. However, how do we constructively apply this theorem to a given Hamiltonian system? The Melnikov method provides a constructive way of proving the hypothesis of transversal intersection between  $W^u(\tilde{x})$  and  $W^s(\tilde{x})$  in the Smale-Birkhoff homoclinic theorem. But this requires the knowledge of a homoclinic, or heteroclinic, loop formed by the  $W^s(\tilde{x})$  and  $W^u(\tilde{x})$  of a hyperbolic stationary solution  $\tilde{x}$ . For Hamiltonian flows of the quasi-integrable type, that is, described by a Hamiltonian of the form  $H(\boldsymbol{\alpha}, \mathbf{J}) = H_0(\mathbf{J}) + \varepsilon H_1(\boldsymbol{\alpha}, \mathbf{J})$ , where  $(\boldsymbol{\alpha}, \mathbf{J})$  are action-angle coordinates, after the Poincaré-Birkhoff theorem [12] the resonant tori of the integrable part  $H_0(\mathbf{J})$  are broken by  $H_1(\boldsymbol{\alpha}, \mathbf{J})$  into an even number of fixed points half of which are hyperbolic and originate heteroclinic loops with unavoidable homoclinic intersections. In any case, the Smale-Birkhoff theorem of course applies to Hamiltonian flows and even if from a theoretical physics viewpoint we assume that homoclinic tangles are *bona fide* always present in phase space of nonintegrable Hamiltonian systems, this is not very satisfactory. In fact, it does not provide an explicit evidence of what causes chaos, and leaves aside any attempt at constructively relating an explanation of the origin of chaos to the way of quantifying its strength through  $\lambda_1$ . In this respect, the Riemannian geometric approach to Hamiltonian chaos has some advantages. It provides, loosely speaking, a "natural" explanation of the origin of chaos because a Hamiltonian flow is easily identified with a geodesic flow, because the Jacobi-Levi-Civita equation for geodesic spread is a powerful tool to investigate the stability of a geodesic flow by relating its stability/instability to the curvature landscape of the mechanical manifolds, landscape which is shaped by the physical potential entering the metric. Finally, "natural" because it makes use of the physical coordinates and momenta without any need to make coordinate transformations like, for instance, to action-angle variables. At the same time, for many-body systems the geometric approach allowed to develop, so to speak, a statistical theory of chaos [13] that can yield to analytical computations of the largest Lyapunov exponent thus providing at the same time an explanation of the origin of chaos and a constructive method to compute its strength. Another remarkable result brought about by the geometric approach is the formulation of a differential-topological theory of phase transitions. This has been spawned by tackling the

Hamiltonian dynamical counterpart of a phase transition in the light of the Riemannian geometrization of the dynamics. This combination has led to discover that in correspondence of a phase transition there are peculiar geometrical changes of the mechanical manifolds that stem from changes of their topology. This has paved the way to a topological theory of phase transitions that goes beyond the existing theories on this topic [11] and that successfully applies to a broad class of systems, also at small  $N$  (systems at nanoscopic and mesoscopic scales), and in the absence of symmetry-breaking.

### III. EISENHART GEOMETRIZATION OF HAMILTONIAN DYNAMICS

It is worth summarizing some basic facts of a geometrization of Hamiltonian dynamics which makes a direct and unexpected link between the standard tangent dynamics equations, used to numerically compute Lyapunov exponents, and the JLC equation for the geodesic spread [11].

#### III.1. Eisenhart Metric on Enlarged Configuration Space-Time $M \times \mathbb{R}^2$

L.P.Eisenhart proposed a geometric formulation of Newtonian dynamics that makes use, as ambient space, of an enlarged configuration space-time  $M \times \mathbb{R}^2$  of local coordinates  $(q^0, q^1, \dots, q^i, \dots, q^N, q^{N+1})$ . This space can be endowed with a nondegenerate pseudo-Riemannian metric [14] whose arc length is

$$ds^2 = (g_e)_{\mu\nu} dq^\mu dq^\nu = a_{ij} dq^i dq^j - 2V(q)(dq^0)^2 + 2dq^0 dq^{N+1}, \quad (8)$$

where  $\mu$  and  $\nu$  run from 0 to  $N+1$  and  $i$  and  $j$  run from 1 to  $N$ . The relation between the geodesics of this manifold and the natural motions of the dynamical system is contained in the following theorem [15]:

**Theorem.** *The natural motions of a Hamiltonian dynamical system are obtained as the canonical projection of the geodesics of  $(M \times \mathbb{R}^2, g_e)$  on the configuration space-time,  $\pi : M \times \mathbb{R}^2 \mapsto M \times \mathbb{R}$ . Among the totality of geodesics, only those whose arc lengths are positive definite and are given by*

$$ds^2 = c_1^2 dt^2 \quad (9)$$

*correspond to natural motions; the condition (9) can be equivalently cast in the following*

integral form as a condition on the extra coordinate  $q^{N+1}$ :

$$q^{N+1} = \frac{c_1^2}{2}t + c_2^2 - \int_0^t L d\tau , \quad (10)$$

where  $c_1$  and  $c_2$  are given real constants. Conversely, given a point  $P \in M \times \mathbb{R}$  belonging to a trajectory of the system, and given two constants  $c_1$  and  $c_2$ , the point  $P' = \pi^{-1}(P) \in M \times \mathbb{R}^2$ , with  $q^{N+1}$  given by (10), describes a geodesic curve in  $(M \times \mathbb{R}^2, g_e)$  such that  $ds^2 = c_1^2 dt^2$ .

For the full proof, see [15]. Since the constant  $c_1$  is arbitrary, we will always set  $c_1^2 = 1$  in order that  $ds^2 = dt^2$  on the physical geodesics.

From (8) it follows that the explicit table of the components of the Eisenhart metric is given by

$$g_e = \begin{pmatrix} -2V(q) & 0 & \cdots & 0 & 1 \\ 0 & a_{11} & \cdots & a_{1N} & 0 \\ \vdots & \vdots & \ddots & \vdots & \vdots \\ 0 & a_{N1} & \cdots & a_{NN} & 0 \\ 1 & 0 & \cdots & 0 & 0 \end{pmatrix} , \quad (11)$$

where  $a_{ij}$  is the kinetic energy metric. The Christoffel coefficients

$$\Gamma_{jk}^i = \frac{1}{2} g^{im} \left( \frac{\partial g_{mk}}{\partial q^j} + \frac{\partial g_{mj}}{\partial q^k} - \frac{\partial g_{jk}}{\partial q^m} \right) \quad (12)$$

for  $g_e$  and with  $a_{ij} = \delta_{ij}$  are found to be non-vanishing only in the following cases

$$\Gamma_{00}^i = -\Gamma_{0i}^{N+1} = \partial_i V , \quad (13)$$

where  $\partial_i = \partial/\partial q^i$  so that the geodesic equations read

$$\frac{d^2 q^0}{ds^2} = 0 , \quad (14)$$

$$\frac{d^2 q^i}{ds^2} + \Gamma_{00}^i \frac{dq^0}{ds} \frac{dq^0}{ds} = 0 , \quad (15)$$

$$\frac{d^2 q^{N+1}}{ds^2} + \Gamma_{0i}^{N+1} \frac{dq^0}{ds} \frac{dq^i}{ds} = 0 ; \quad (16)$$

using  $ds = dt$  one obtains

$$\frac{d^2 q^0}{dt^2} = 0 , \quad (17)$$

$$\frac{d^2 q^i}{dt^2} = -\frac{\partial V}{\partial q_i} , \quad (18)$$

$$\frac{d^2 q^{N+1}}{dt^2} = -\frac{dL}{dt} . \quad (19)$$

Equation (17) states only that  $q^0 = t$ . The  $N$  equations (18) are Newton's equations, and (19) is the differential version of (10).

The fact that in the framework of the Eisenhart metric the dynamics can be geometrized with an affine parametrization of the arc length, i.e.,  $ds = dt$ , will be extremely useful in the following, together with the remarkably simple curvature properties of the Eisenhart metric.

### III.1.1. Curvature of $(M \times \mathbb{R}^2, g_e)$

The curvature properties of the Eisenhart metric  $g_e$  are much simpler than those of the Jacobi metric, and this is obviously a great advantage from a computational point of view. The components of the Riemann–Christoffel curvature tensor are

$$R^k_{ijr} = (\Gamma^t_{ri}\Gamma^k_{jt} - \Gamma^t_{ji}\Gamma^k_{rt} + \partial_j\Gamma^k_{ri} - \partial_r\Gamma^k_{ji}) . \quad (20)$$

Hence, and after Eq.(13), the only non-vanishing components of the curvature tensor are

$$R_{0i0j} = \partial_i\partial_j V \quad (21)$$

hence the Ricci tensor has only one nonzero component

$$R_{00} = \Delta V \quad (22)$$

so that the Ricci curvature is

$$K_R(q, \dot{q}) = R_{00}\dot{q}^0\dot{q}^0 \equiv \Delta V , \quad (23)$$

and the scalar curvature is identically vanishing  $\mathcal{R}(q) = 0$  .

### III.1.2. Geodesic Spread Equation for the Eisenhart Metric $g_e$

The Jacobi equation (3) for  $(M \times \mathbb{R}^2, g_e)$  takes the form

$$\frac{\nabla^2 J^0}{ds^2} + R^0_{i0j} \frac{dq^i}{ds} J^0 \frac{dq^j}{ds} + R^0_{0ij} \frac{dq^0}{ds} J^i \frac{dq^j}{ds} = 0 , \quad (24)$$

$$\frac{\nabla^2 J^i}{ds^2} + R^i_{0j0} \left( \frac{dq^0}{ds} \right)^2 J^j + R^i_{00j} \frac{dq^0}{ds} J^0 \frac{dq^j}{ds} + R^i_{j00} \frac{dq^j}{ds} J^0 \frac{dq^0}{ds} = 0 , \quad (25)$$

$$\frac{\nabla^2 J^{N+1}}{ds^2} + R^{N+1}_{i0j} \frac{dq^i}{ds} J^0 \frac{dq^j}{ds} + R^{N+1}_{ij0} \frac{dq^i}{ds} J^j \frac{dq^0}{ds} = 0 , \quad (26)$$

and since  $\Gamma_{ij}^0 = 0$  and  $\Gamma_{0k}^i = 0$  it is  $\nabla J^0/ds = dJ^0/ds$ ,  $R_{ijk}^0 = 0$ , and  $\nabla J^i/ds = dJ^i/ds$ , the only accelerating components of the vector field  $J$  are found to obey the equations

$$\frac{d^2 J^i}{ds^2} + \frac{\partial^2 V}{\partial q_i \partial q^k} \left( \frac{dq^0}{ds} \right)^2 J^k = 0 . \quad (27)$$

and using  $dq^0/ds = 1$  one is left with

$$\frac{d^2 J^i}{dt^2} + \frac{\partial^2 V}{\partial q_i \partial q^k} J^k = 0 , \quad (28)$$

the usual tangent dynamics equations. This fact is a crucial point in the development of a geometric theory of Hamiltonian chaos because there is no new definition of chaos in the geometric context. In fact, the numerical Lyapunov exponents computed by means of Eqs.(28) already belong to geometric treatment of chaotic geodesic flows.

### III.2. Eisenhart Metric on Configuration Space-Time $M \times \mathbb{R}$

Another interesting choice of the ambient space and Riemannian metric to reformulate Newtonian dynamics in a geometric language was also proposed by Eisenhart [14]. If and how the description of Hamiltonian chaos in this framework is coherent with the results obtained by standard treatment based on the tangent-dynamics/JLC equations discussed in the preceding section has never been investigated before.

This geometric formulation makes use of an enlarged configuration space  $M \times \mathbb{R}$ , with local coordinates  $(q^0, q^1, \dots, q^N)$ , where a proper Riemannian metric  $G_e$  is defined to give

$$ds^2 = (G_e)_{\mu\nu} dq^\mu dq^\nu = a_{ij} dq^i dq^j + A(q) (dq^0)^2 , \quad (29)$$

where  $\mu$  and  $\nu$  run from 0 to  $N$  and  $i$  and  $j$  run from 1 to  $N$ , and the function  $A(q)$  does not explicitly depend on time. With the choice  $1/[2A(q)] = V(q) + \eta$  and under the condition

$$q^0 = 2 \int_0^t V(q) d\tau + 2\eta t , \quad (30)$$

for the extra variable it can easily be seen that the geodesics of the manifold  $(M \times \mathbb{R}, G_e)$  are the natural motions of standard autonomous Hamiltonian systems. Since  $\frac{1}{2}a_{ij}\dot{q}^i\dot{q}^j + V(q) = E$ , where  $E$  is the energy constant along a geodesic, we can see that the following relation exists between  $q^0$  and the action:

$$q^0 = -2 \int_0^t T d\tau + 2(E + \eta)t . \quad (31)$$

Explicitly, the metric  $G_e$  reads as

$$G_e = \begin{pmatrix} [2V(q) + 2\eta]^{-1} & 0 & \cdots & 0 \\ 0 & a_{11} & \cdots & a_{1N} \\ \vdots & \vdots & \ddots & \vdots \\ 0 & a_{N1} & \cdots & a_{NN} \end{pmatrix}, \quad (32)$$

and together with the condition (31), this gives an affine parametrization of the arc length with the physical time, i.e.,  $ds^2 = 2(E + \eta)dt^2$ , along the geodesics that coincide with natural motions. The constant  $\eta$  can be set equal to an arbitrary value greater than the largest value of  $|E|$  so that the metric  $G_e$  is nonsingular. This metric is a priori very interesting because it seems to have some better property than the Jacobi metric and than the previous metric  $g_e$ . In fact, at variance with the Jacobi metric  $g_J$  in Eq.(6), the metric  $G_e$  is nonsingular on the boundary  $V(q) = E$ ; moreover, by varying the total energy  $E$  we get a family of different metrics  $g_J$ , whereas by choosing a convenient value of  $\eta$ , at different values of the energy the metric  $G_e$  remains the same. The consequence is that a comparison among the geometries of the submanifolds of  $(M \times \mathbb{R}, G_e)$ —where the geodesic flows of different energies “live”—is meaningful. To the contrary, this is not true with  $(M_E, g_J)$ . In some cases, the possibility of making this kind of comparison can be important. With respect to the Eisenhart metric  $g_e$  on  $M \times \mathbb{R}^2$  in the previous section, the metric  $G_e$  on  $M \times \mathbb{R}$  defines a somewhat richer geometry, for example the scalar curvature of  $g_e$  is identically vanishing, which is not the case of  $G_e$ .

In the case of a diagonal kinetic-energy metric, i.e.  $a_{ij} \equiv \delta_{ij}$ , the only non vanishing Christoffel symbols are

$$\Gamma_{00}^i = \frac{(\partial V / \partial q^i)}{[2V(q) + 2\eta]^2}, \quad \Gamma_{i0}^0 = -\frac{(\partial V / \partial q^i)}{[2V(q) + 2\eta]}, \quad (33)$$

whence the geodesic equations

$$\frac{d^2 q^0}{ds^2} + \Gamma_{i0}^0 \frac{dq^i}{ds} \frac{dq^0}{ds} + \Gamma_{0i}^0 \frac{dq^0}{ds} \frac{dq^i}{ds} = 0, \quad (34)$$

$$\frac{d^2 q^i}{ds^2} + \Gamma_{00}^i \frac{dq^0}{ds} \frac{dq^0}{ds} = 0, \quad (35)$$

which, using the affine parametrization of the arc length with time, i.e.,  $ds^2 = 2(E + \eta)dt^2$ ,

with  $(dq^0/dt) = 2[V(q) + \eta]$  from (30), give

$$\begin{aligned}\frac{d^2 q^0}{dt^2} &= 2 \frac{dV}{dt} , \\ \frac{d^2 q^i}{dt^2} &= -\frac{\partial V}{\partial q_i}, \quad i = 1, \dots, N ,\end{aligned}\tag{36}$$

respectively. The first equation is the differential version of (30), and equations (36) are Newton's equations of motion.

### III.2.1. Curvature of $(M \times \mathbb{R}, G_e)$

The basic curvature properties of the Eisenhart metric  $G_e$  can be derived by means of the Riemann curvature tensor, which is found to have the non-vanishing components

$$R_{0i0j} = \frac{\partial_i \partial_j V}{(2V + 2\eta)^2} - \frac{3(\partial_i V)(\partial_j V)}{(2V + 2\eta)^3} ,\tag{37}$$

whence, after contraction, using  $G^{00} = 2V + 2\eta$  the components of the Ricci tensor are found to be

$$\begin{aligned}R_{kj} &= \frac{\partial_k \partial_j V}{(2V + 2\eta)} - \frac{3(\partial_k V)(\partial_j V)}{(2V + 2\eta)^2} , \\ R_{00} &= \frac{\Delta V}{(2V + 2\eta)^2} - \frac{3\|\nabla V\|^2}{(2V + 2\eta)^3} ,\end{aligned}\tag{38}$$

where  $\Delta V = \sum_{i=1}^N \partial^2 V / \partial q^{i^2}$ , and thus we find that the Ricci curvature at the point  $q \in M \times \mathbb{R}$  and in the direction of the velocity vector  $\dot{q}$  is

$$K_R(q, \dot{q}) = \Delta V + R_{ij} \dot{q}^i \dot{q}^j\tag{39}$$

and the scalar curvature at  $q \in M \times \mathbb{R}$  is

$$\mathcal{R}(q) = \frac{\Delta V}{(2V + 2\eta)} - \frac{3\|\nabla V\|^2}{(2V + 2\eta)^2} .\tag{40}$$

### III.2.2. Geodesic Spread Equation for the Eisenhart Metric $G_e$

Let us now give the explicit form of Eq.(3) in the case of  $(M \times \mathbb{R}, G_e)$ , the enlarged configuration space-time equipped with one of the Eisenhart metrics. Since the nonvanishing



Christoffel coefficients are  $\Gamma_{00}^i$  and  $\Gamma_{0i}^0$ , then using the affine parametrization of the arc length with physical time, we obtain

$$\begin{aligned} \frac{d^2 J^k}{dt^2} + \frac{2(\partial_k V)}{2V + 2\eta} \frac{dJ^0}{dt} + \left[ \partial_{kj}^2 V - \frac{4(\partial_k V)(\partial_j V)}{2V + 2\eta} \right] J^j &= 0, \\ \frac{d^2 J^0}{dt^2} - \frac{2(\partial_i V)\dot{q}^i}{2V + 2\eta} \frac{dJ^0}{dt} - 2(\partial_i V) \frac{dJ^i}{dt} - \left[ \partial_{ij}^2 V - \frac{2(\partial_i V)(\partial_j V)}{2V + 2\eta} \right] \dot{q}^i J^j &= 0, \end{aligned} \quad (41)$$

where the indexes  $i, j, k$  run from 1 to  $N$ . These equations have not yet been used to tackle Hamiltonian chaos, but are certainly worth to be investigated. As reported in Ref.[19], the JLC equation in Eq.(7) is rather complicated for the kinetic energy (Jacobi) metric in (6), it considerably simplifies to (28) for  $(M \times \mathbb{R}^2, g_e)$ , and displays an intermediate level of complexity for  $(M \times \mathbb{R}, G_e)$  as shown by Eqs.(41). This is related with a different degree of "richness" of the geometrical properties of the respective manifolds. It is therefore important to check whether all these geometrical frameworks provide the same information about regular and chaotic motions [17–19], a necessary condition which a-priori could be questioned as it was done in Ref.[16] even though the claims of this work have been proved wrong in [20].

#### IV. ORDER AND CHAOS IN A PARADIGMATIC TWO-DEGREES OF FREEDOM MODEL WITH $(M \times \mathbb{R}, G_e)$

The first benchmarking is performed for a two-degrees of freedom system. In this case a paradigmatic candidate is the Hénon-Heiles model described by the Hamiltonian

$$H = \frac{1}{2} (p_x^2 + p_y^2) + \frac{1}{2} (q_1^2 + q_2^2) + q_1^2 q_2 - \frac{1}{3} q_2^3. \quad (42)$$

In this case, the JLC equation for the Jacobi metric is exactly written in the form

$$\frac{d^2 J^\perp}{ds^2} + \frac{1}{2} \left[ \frac{\Delta V}{(E - V)^2} + \frac{\|\nabla V\|^2}{(E - V)^3} \right] J = 0, \quad (43)$$

$$\frac{d^2 J^\parallel}{ds^2} = 0 \quad (44)$$

where the expression in square brackets is the scalar curvature of the manifold  $(M_E, g_J)$ ,  $g_J$  is the metric tensor whose components are in Eq.(6),  $J^\perp$  and  $J^\parallel$  are the components of the geodesic separation vector transversal and parallel to the velocity vector along the reference geodesic, respectively. It is well evident that this scalar curvature is always positive and that

chaotic motions can only be the consequence of parametric instability due to the variability of the scalar curvature along the geodesics. At first sight, the scalar curvature of  $(M \times \mathbb{R}, G_e)$  given in Eq.(40) can take also negative values as is shown in Figure 1. On the one side this could add another source of dynamical instability to parametric instability, but, on the other side, the extension of regions of negative curvature depends on the value of the arbitrary parameter  $\eta$  that enters the metric  $G_e$ , extension that can be arbitrarily reduced making its contribution to degree of chaoticity not intrinsic. In Figure 2 the plane  $(q_1, q_2)$  is taken as surface of section of phase space trajectories when  $p_2 = 0$  and  $p_1 > 0$ .

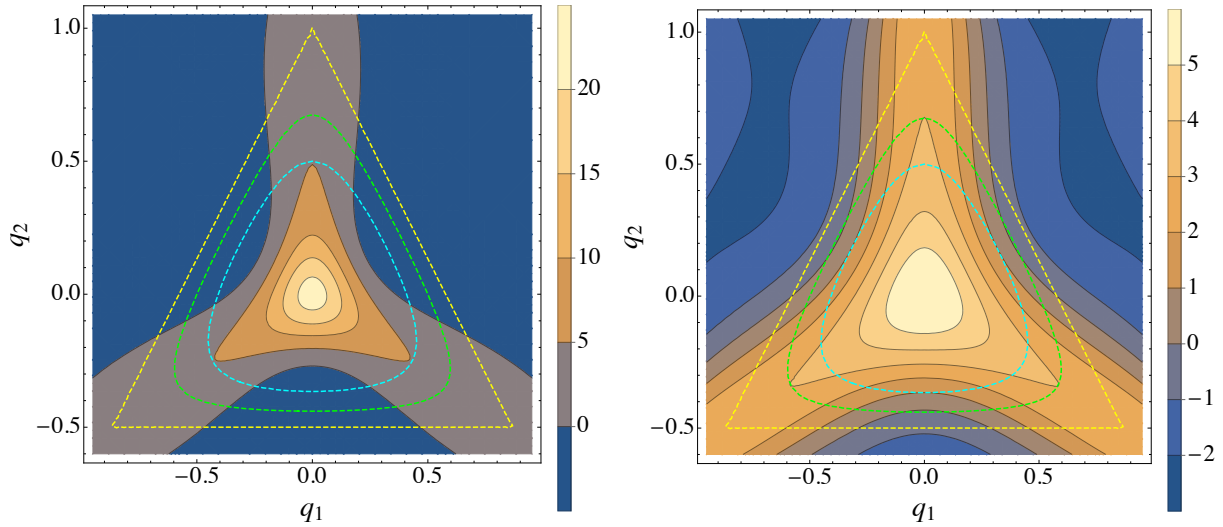


FIG. 1. Configuration space of the Hénon-Heiles model. The dashed lines represent the equipotential boundaries:  $V(q_1, q_2) = 0.0833$  (cyan);  $V(q_1, q_2) = 0.125$  (green);  $V(q_1, q_2) = 0.1667$  (yellow). Left panel:  $\eta = 0.045$ . Right panel:  $\eta = 0.1667$ . The scale of colours represents different intervals of values of the scalar curvature given in Eq.(40).

At the lowest energy,  $E = 0.0833$ , when all the motions are regular, the trajectories are found to visit also regions of negative curvature, whereas at higher energies,  $E = 0.125$  and  $E = 0.1667$ , the chaotic trajectories considered display a large number of intersections in regions of positive curvature. In other words, the role of negatively curved regions does not appear to play a relevant role in determining the chaotic instability of the dynamics.

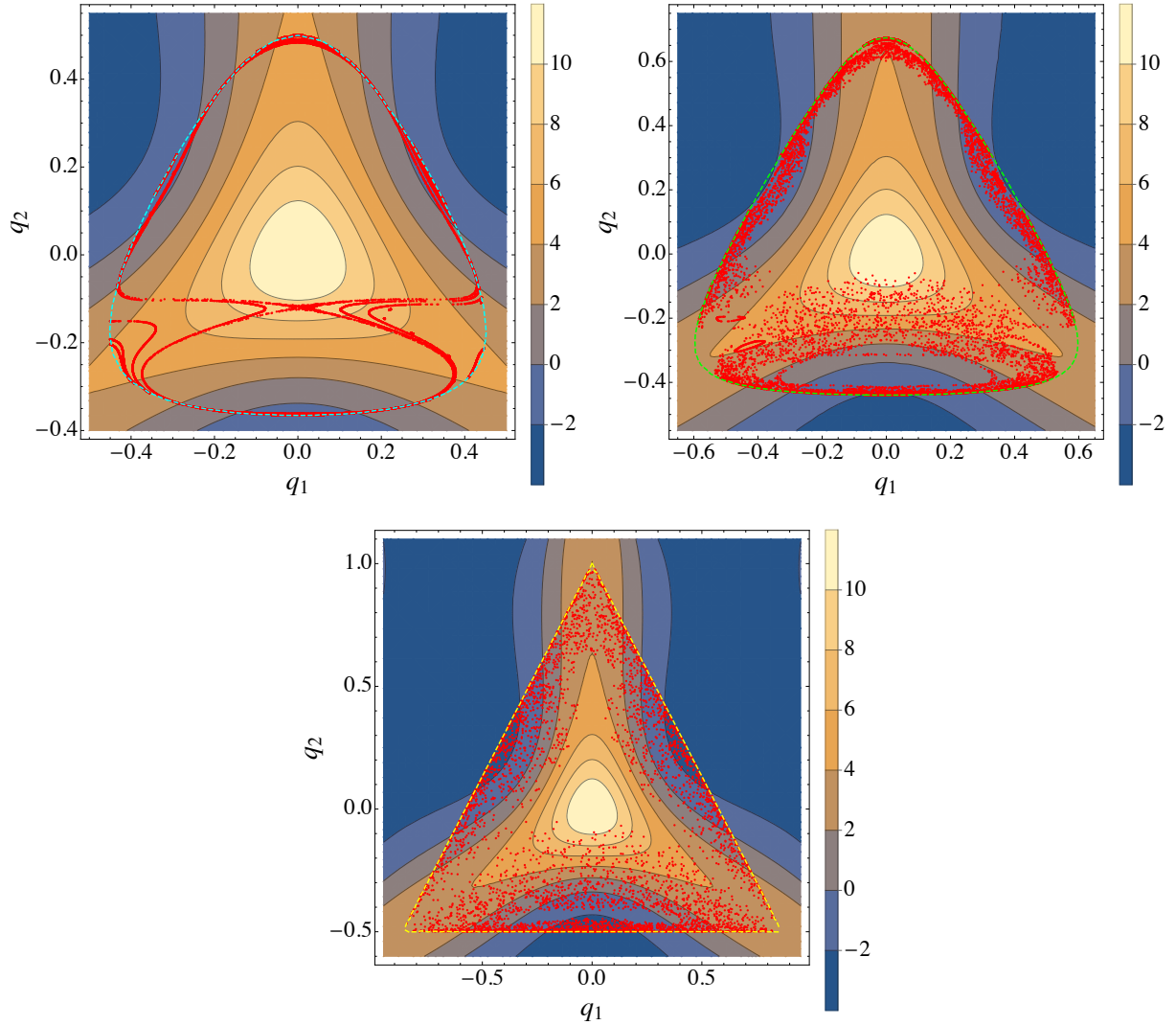


FIG. 2. Superposition of the configuration space of the Hénon-Heiles model with the surfaces of section of phase space trajectories. Red dots correspond to the crossing of the  $(q_1, q_2)$  plane when  $p_2 = 0$  and  $p_1 > 0$ . Upper left panel corresponds to  $E = 0.0833$ ; upper right panel corresponds to  $E = 0.125$ ; lower panel corresponds to  $E = 0.1667$ . For all these cases  $\eta = 0.0833$ .

As a matter of fact, the comparison of the results obtained by numerically integrating the stability equations (28), (41), and (43) along with the equations of motion of the Hénon-Heiles model, at different energies and initial conditions, show an excellent qualitative and quantitative agreement. The integration of the Hamilton equations of motion is performed with a symplectic integrator and the stability equations have been integrated with a fourth-order Runge-Kutta scheme (see Appendix A for details). The choice of the energy values

follows the historical paper by Hénon-Heiles, and the initial conditions for regular and chaotic motions are chosen according to the selections in Ref.[18]. The quantity reported in Figures 3 and 4 is

$$\lambda(t) = \frac{1}{t} \log \left[ \frac{\|\dot{J}(t)\|^2 + \|J(t)\|^2}{\|\dot{J}(0)\|^2 + \|J(0)\|^2} \right] \quad (45)$$

where the separation vector  $J$  is in turn the solution of the three different stability equations.

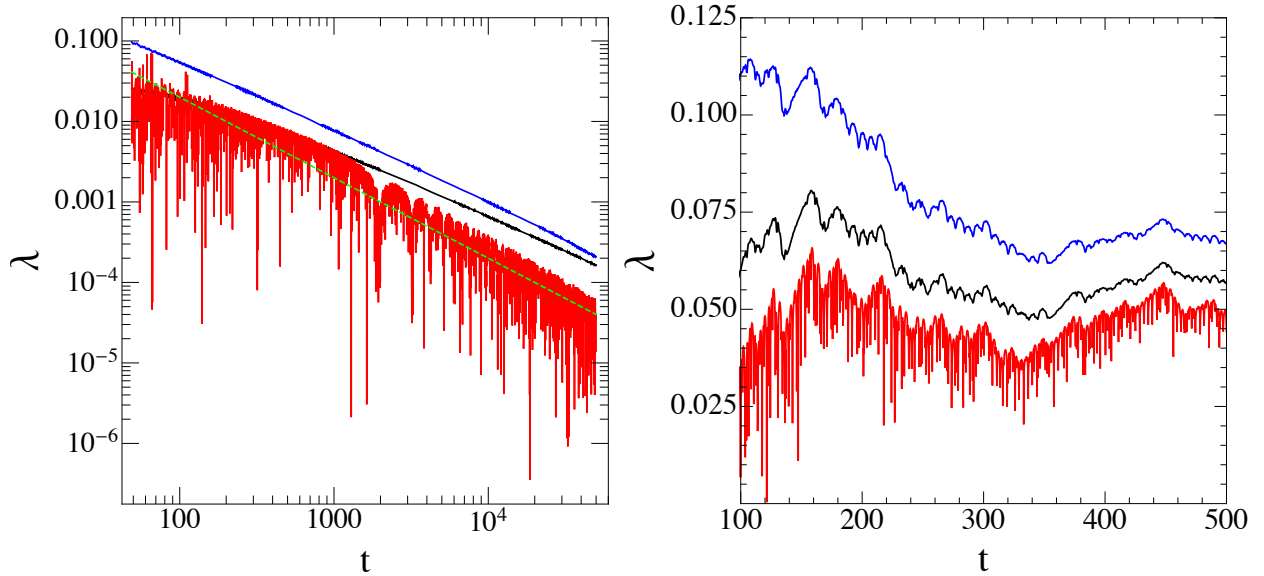


FIG. 3. Numerical solutions of the tangent dynamics equation (28) (black line) compared to the solution of equation (41) (blue line), and to the solution of equation (43) (red line). Left panel:  $E = 0.0833$ ,  $\eta = 0.0833$  and the initial condition is point (a) of Figure 1 of [18]. The dashed green line is the reference  $t^{-1}$  slope for regular motions. Right panel:  $E = 0.125$ ,  $\eta = 0.0833$  and the initial condition is point (d) of Figure 3 of [18].

The robustness of the results obtained by means of Eq.(41) for the manifold  $(M \times \mathbb{R}, G_e)$  with respect to different choices of the free parameter  $\eta$  has been checked and confirmed. It is in particular the close agreement between the results obtained with the Eqs.(41) and (43) which confirms that chaos stems from parametric instability, because in the latter equation the scalar curvature is always positive. The right panel of Figure 3 shows a clear qualitative agreement among the three patterns  $\lambda(t)$  but some quantitative deviations that do not change neither with longer integrations nor by changing the value of  $\eta$  in the case of  $\lambda(t)$  computed with (41). Perhaps such a discrepancy could stem from the inhomogeneity of the chaotic layer in phase space due to the presence of very small regular islands, inhomogeneity

detected differently by the different JLC equations. Actually, this discrepancy is no longer observed at higher energy (right panel of Figure 4) when the chaotic layer seems more homogeneous. The reason why the geometrization of Hamiltonian dynamics by means of  $(M \times \mathbb{R}, G_e)$  can be of prospective interest relies on its intermediate geometrical "richness".

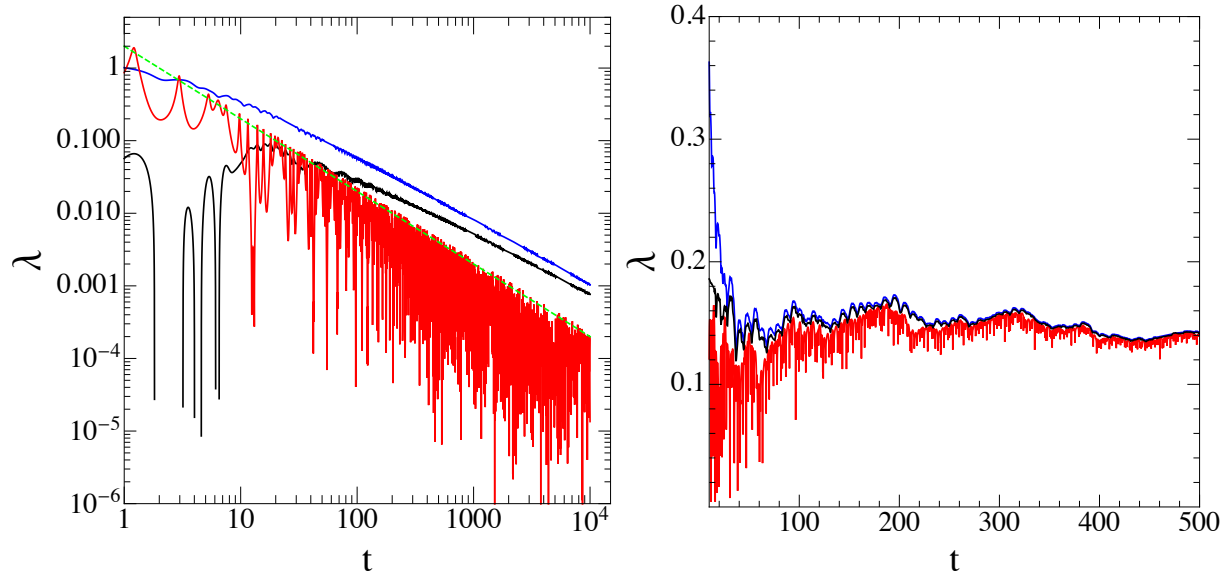


FIG. 4. Numerical solutions of the tangent dynamics equation (28) (black line) compared to the solution of equation (41) (blue line), and to the solution of equation (43) (red line). Here  $E = 0.1667$ ,  $\eta = 0.0833$  and the initial condition for the left panel is point (a) of Figure 5 of [18], and for the right panel point ( $c_2$ ) of the same Figure.

On  $(M \times \mathbb{R}^2, g_e)$  the scalar curvature is always vanishing, the Riemann curvature tensor is just the Hessian of the potential and the Ricci tensor has only one non-vanishing component, to the opposite, on  $(M_E, g_J)$  the Riemann curvature tensor has  $\mathcal{O}(N^4)$  non-vanishing components and at large  $N$  the scalar curvature can happen to be overwhelmingly negative without affecting the degree of chaoticity of the dynamics. The geometry of  $(M \times \mathbb{R}, G_e)$  is definitely richer than that of  $(M \times \mathbb{R}^2, g_e)$  and less complicated than that of  $(M_E, g_J)$ , therefore, and mainly at large  $N$ , this framework can offer some computational advantage for more refined investigations about the geometric origin of parametric instability of the geodesics. Loosely speaking, to give an idea of what a more refined geometrical investigation might mean, it has been shown [11, 22] that integrability is related with the existence of Killing tensor fields on the mechanical manifolds, therefore the degree of breaking of the

hidden symmetries associated with Killing tensor fields could be defined, investigated, and related with the existence of weak and strong chaos in Hamiltonian flows.

## V. ONE-DIMENSIONAL $XY$ -MODEL IN THE EISENHART METRIC $(M \times \mathbb{R}, G_e)$

Let us now proceed to investigate how Hamiltonian chaos is described in this geometric framework at a large number of degrees of freedom. This is shown for a specific model, the one-dimensional classical  $XY$  model. The reason for choosing this model is that it has a rich variety of dynamical behaviors: at low energy it is equivalent to a collection of weakly coupled harmonic oscillators, at asymptotically high energy it represents a set of freely rotating spins, at intermediate energies it displays a strongly chaotic dynamics, as witnessed by the whole spectrum of Lyapounov exponents [21]. Moreover, for this model it was necessary to introduce an *ad hoc* adjustment of an otherwise successful geometric-statistical model for the analytic computation of the largest Lyapounov exponent [13] carried on in the framework  $(M \times \mathbb{R}^2, g_e)$ . It is thus interesting to check whether or not another geometric framework can allow to fix the problem more naturally.

The 1D  $XY$  model, describes a linear chain of  $N$  spins/rotators constrained to rotate in a plane and coupled by a nearest-neighbour interaction. This model is formally obtained by restricting the classical Heisenberg model with  $O(2)$  symmetry to one spatial dimension. The potential energy of the  $O(2)$  Heisenberg model is  $V = -\mathcal{J} \sum_{\langle i,j \rangle} \mathbf{s}_i \cdot \mathbf{s}_j$ , where the sum is extended only over nearest-neighbour pairs,  $\mathcal{J}$  is the coupling constant, and each  $\mathbf{s}_i$  has unit modulus and rotates in the plane. To each “spin”  $\mathbf{s}_i = (\cos q_i, \sin q_i)$ , the velocity  $\dot{\mathbf{s}}_i = (-\dot{q}_i \sin q_i, \dot{q}_i \cos q_i)$  is associated, so that  $H = \sum_{i=1}^N \frac{1}{2} \dot{\mathbf{s}}_i^2 - \mathcal{J} \sum_{\langle i,j \rangle} \mathbf{s}_i \cdot \mathbf{s}_j$ . The Hamiltonian of this model is then

$$H(p, q) = \sum_{i=1}^N \frac{p_i^2}{2} + \mathcal{J} \sum_{i=1}^N [1 - \cos(q_i - q_{i-1})] , \quad (46)$$

The canonical coordinates  $q_i$  and  $p_i$  are thus given the meaning of angular coordinates and momenta. As already mentioned above, this Hamiltonian system has two integrable limits. In the low-energy limit it represents a chain of harmonic oscillators, as can be seen by

expanding the potential energy in power series

$$H(p, q) \approx \sum_{i=1}^N \left[ \frac{p_i^2}{2} + \frac{\mathcal{J}}{2} (q_{i+1} - q_i)^2 \right], \quad (47)$$

where  $p_i = \dot{q}_i$ , whereas in the high-energy limit it represents a system of freely rotating objects, since the kinetic energy increases with total energy without bounds, at variance with potential energy which is bounded from above.

### V.1. Numerical solution of the JLC equation for $(M \times \mathbb{R}, G_e)$

Let us proceed by comparing the outcomes of the integration of the equations (28) and (41) computed along the flow of the Hamiltonian (46). The standard tangent dynamics equations (28) can be split as

$$\begin{aligned} \dot{J}_q^i &= J_p^i \\ \dot{J}_p^i &= -\frac{\partial^2 V}{\partial q_i \partial q^j} J_q^j \end{aligned} \quad (48)$$

which explicitly read as

$$\begin{aligned} \dot{J}_q^i &= J_p^i \\ \dot{J}_p^i &= -\mathcal{J} \cos(q_{i-1} - q_i) J_q^{i-1} + \mathcal{J} [\cos(q_{i-1} - q_i) + \cos(q_i - q_{i+1})] J_q^i - \mathcal{J} \cos(q_i - q_{i+1}) J_q^{i+1}, \end{aligned} \quad (49)$$

whence the Largest Lyapunov Exponent is worked out by computing

$$\lambda_1 = \lim_{t \rightarrow \infty} \frac{1}{t} \log \left[ \frac{\|J_q(t)\|^2 + \|\dot{J}_p(t)\|^2}{\|J_q(0)\|^2 + \|\dot{J}_p(0)\|^2} \right]. \quad (50)$$

At the same time, the integration of the JLC equations (41), by setting  $J = (J^0, J^i)$ , and choosing  $\eta = E$ , yields another estimate of the instability exponent through the analogous definition

$$\lambda_G = \lim_{t \rightarrow \infty} \frac{1}{t} \log \left[ \frac{\|J(t)\|_{G_e}^2 + \|\dot{J}(t)\|_{G_e}^2}{\|J(0)\|_{G_e}^2 + \|\dot{J}(0)\|_{G_e}^2} \right]. \quad (51)$$

We have solved the equations of motion of the 1D  $XY$  model (setting  $\mathcal{J} = 1$ ) and the tangent dynamics equations (49) by using a bi-lateral symplectic algorithm [23]. The JLC equations (41) have been solved by using a third-order predictor-corrector algorithm. Periodic boundary conditions have been considered. Random initial conditions have been adopted by taking the  $q_i$  randomly distributed in the interval  $[0, 2\pi]$ , and by taking the  $p_i$

gaussian-distributed and suitably scaled so as to complement with the kinetic energy the difference between the total energy initially set and the initial value of the potential energy resulting from the random assignment of the  $q_i$ . Figure 5 shows the comparison between the results obtained at different values of the energy density  $\epsilon = E/N$  for  $\lambda_1(\epsilon)$  and  $\lambda_G(\epsilon)$  defined above. It is well evident that the results so obtained are globally in very good agreement. At energy densities in the interval between  $\epsilon \simeq 0.2$  and  $\epsilon \simeq 100$  the agreement is perfect, whereas at lower energy densities, below  $\epsilon \simeq 0.2$ , small discrepancies are found which seem due to a slower time-relaxation of  $\lambda_G(t)$  with respect to  $\lambda_1(t)$ .

Of course, an unavoidable check of consistency has to be performed on an integrable dynamics. This check has been performed on the flow of the Hamiltonian (47). The results obtained with the equations (28) and (41) are reported in Figure (6). As expected for non-chaotic dynamics, it is found that  $\lambda_1(t)$  decays as a straight line of slope  $-1$  in double logarithmic scale, and  $\lambda_G(t)$  decays with an oscillating pattern with a  $t^{-1}$  envelope. This has been checked at different  $N$  and energy values. Some cases are reported in Figure 6.

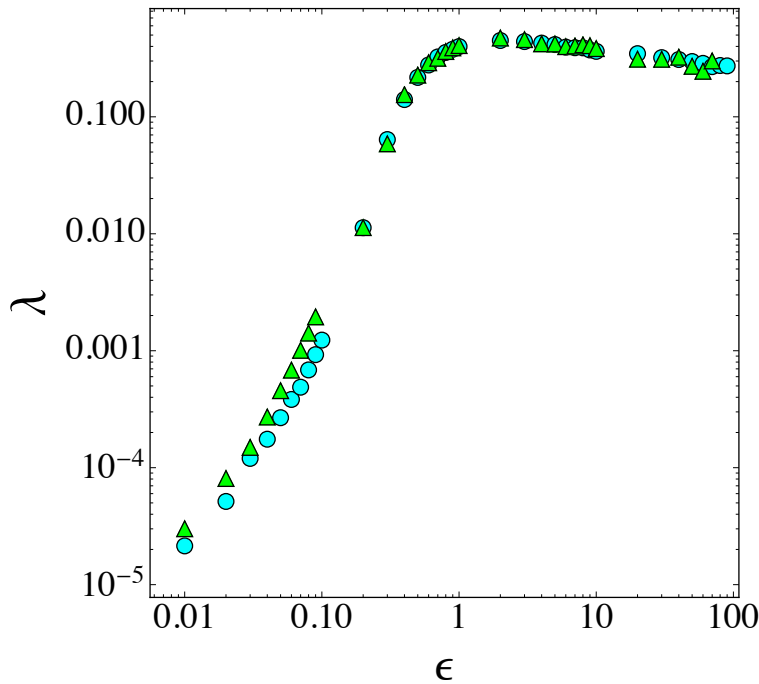


FIG. 5. Lyapunov Exponents  $\lambda_1$  (cyan circles) and  $\lambda_G$  (green triangles) versus the energy density  $\epsilon$  for a system of  $N = 150$  spins. The parameter  $\eta$  has been set as  $\eta = E$ .



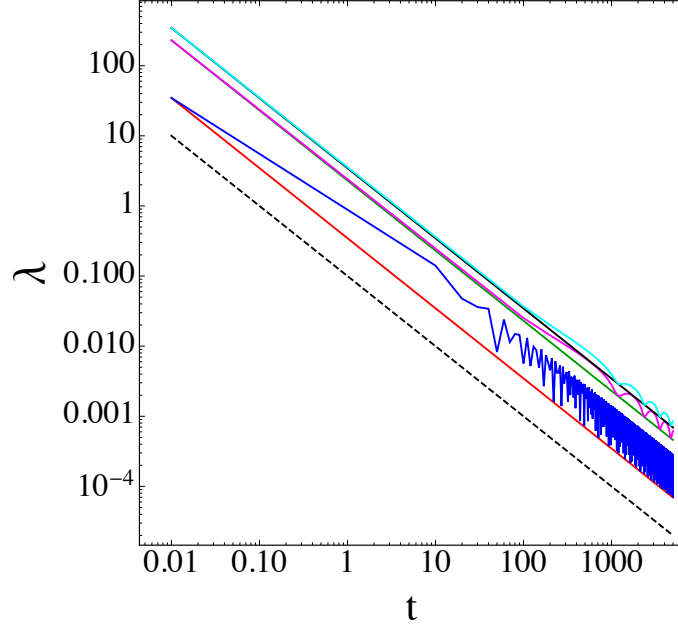


FIG. 6. Lyapunov Exponents  $\lambda_1(t)$  (red, green and black lines) versus  $\lambda_G(t)$  (blue, magenta and cyan lines) for a system of  $N = 2, 100, 1000$  harmonic oscillators, respectively. The black dashed line is the  $t^{-1}$  reference slope for a regular dynamics. Here  $\epsilon = 1$  and  $\eta = E$ .

## VI. THE EFFECTIVE SCALAR MODEL FOR THE JLC EQUATION

In [13] an effective scalar approximation of the JLC equation (7) has been worked out under some suitable hypothesis. In a nutshell, at large  $N$  under an hypothesis of quasi-isotropy - meaning that a coarse-grained mechanical manifold appears as a constant curvature isotropic manifold - with broad spatial spectrum of curvature variations at a finer scale, the evolution of the norm of the geodesic separation vector is described by a stochastic oscillator equation

$$\frac{d^2\psi(s)}{ds^2} + [\langle k_R \rangle + \langle \delta^2 k_R \rangle^{1/2} \eta(s)] \psi(s) = 0$$

where  $\eta(s)$  a  $\delta$ -correlated gaussian stochastic process of zero mean and unit variance, and

$$\begin{aligned} \langle k_R \rangle &= \frac{1}{N-1} \langle K_R \rangle \\ \langle \delta^2 k_R \rangle^{1/2} &= \frac{1}{N-1} (\langle K_R^2 \rangle - \langle K_R \rangle^2) \end{aligned}$$

where  $K_R$  is the Ricci curvature of the mechanical manifold under consideration, and the averages are meant along a reference geodesic or as microcanonical averages on suitable

energy surface  $\Sigma_E$ . By putting  $k_0 = \langle k_R \rangle$ ,  $\sigma = \langle \delta^2 k_R \rangle^{1/2}$ ,

$$\begin{aligned}\tau_1 &= \left\langle \frac{dt}{ds} \right\rangle \frac{\pi}{2\sqrt{k_0 + \sigma}} \\ \tau_2 &= \left\langle \frac{dt}{ds} \right\rangle \frac{k_0^{1/2}}{\sigma}\end{aligned}\tag{52}$$

and hence defining  $\tau^{-1} = 2(\tau_1^{-1} + \tau_2^{-1})$ , an analytic expression for a geometric Largest Lyapunov Exponent is given by [13]

$$\begin{aligned}\lambda(k_0, \sigma, \tau) &= \frac{1}{2} \left( \Lambda - \frac{4k_0}{3\Lambda} \right), \\ \Lambda &= \left( \sigma^2 \tau + \sqrt{\left( \frac{4k_0}{3} \right)^3 + \sigma^4 \tau^2} \right)^{1/3}.\end{aligned}\tag{53}$$

This can be applied to the geometrization on the manifold  $(M \times \mathbb{R}, G_e)$  of Hamiltonian dynamics. In this case the Ricci curvature reads as

$$K_R(s) = \frac{1}{2(E + \eta)} \left( \Delta V - \frac{3\|\nabla V\|^2}{2V + 2\eta} + \frac{\partial_{kj}^2 V \dot{q}^j \dot{q}^k}{2V + 2\eta} - \frac{3\partial_j V \dot{q}^j \partial_k V \dot{q}^k}{(2V + 2\eta)^2} \right) \equiv \frac{K_R(t)}{2(E + \eta)}\tag{54}$$

and using the arc-length parametrization  $ds^2 = 2(E + \eta)dt^2$  with physical time, we can compute by means of Eqs.(53) an analytic prediction of  $\lambda_G(\epsilon)$  for  $(M \times \mathbb{R}, G_e)$  and compare it to the outcome obtained for  $(M \times \mathbb{R}^2, g_e)$ .

The first step consists in computing the average Ricci curvature and its variance of the two manifolds at different values of the energy density. We can limit these computations to one single choice of  $N$  for which the asymptotic values of  $\langle k_R \rangle$  and  $\langle \delta^2 k_R \rangle$  are already attained (see [13]). Moreover, for non-integrable systems, after the Poincaré-Fermi theorem, all the constant energy surface is accessible to the dynamics, and since chaos entails phase space mixing, with sufficiently long integration times we obtain good estimate of microcanonical averages of the observables of interest. Figures 7 and 8 provide the comparison between  $\langle k_R \rangle$  and  $\langle \delta^2 k_R \rangle$  for the two manifolds.

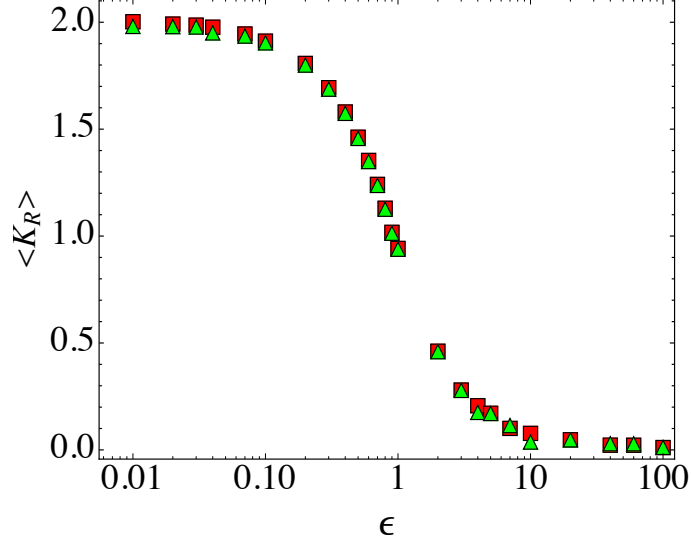


FIG. 7. Average of Ricci curvature  $\langle K_R \rangle$  of  $M \times \mathbb{R}^2$  (red squares) and of  $M \times \mathbb{R}$  (green triangles), respectively, vs energy density  $\epsilon$  for a system of  $N = 150$ . Here  $\eta = E$ .

Somewhat unexpectedly these average quantities are found to be practically coincident, thus it is not surprising that the application of the effective scalar model for the JLC equation - recalled above - yields outcomes in close agreement, as shown by Figure 9.

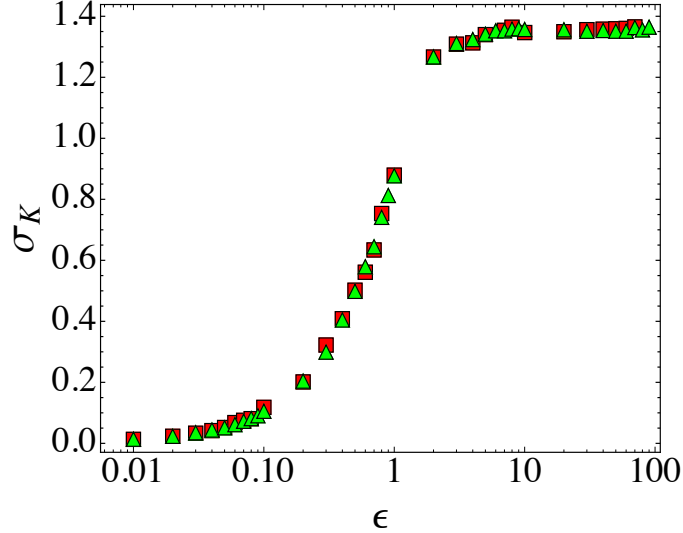


FIG. 8. Average variance of the Ricci curvature  $\sigma_K$  of  $M \times \mathbb{R}^2$  (red squares) and of  $M \times \mathbb{R}$  (green triangles) vs energy density  $\epsilon$  for a system of  $N = 150$  particles. Here  $\eta = E$ .

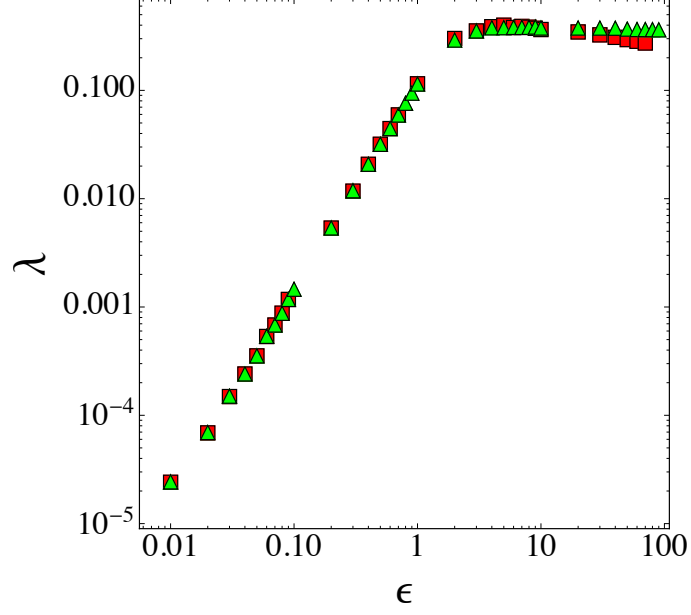


FIG. 9. Geometric Lyapunov Exponents  $\lambda$  worked out for  $M \times \mathbb{R}^2$  (red squares) and for  $M \times \mathbb{R}$  (green triangles) vs energy density  $\epsilon$ , for a system of  $N = 150$  particles. Here  $\eta = E$ .

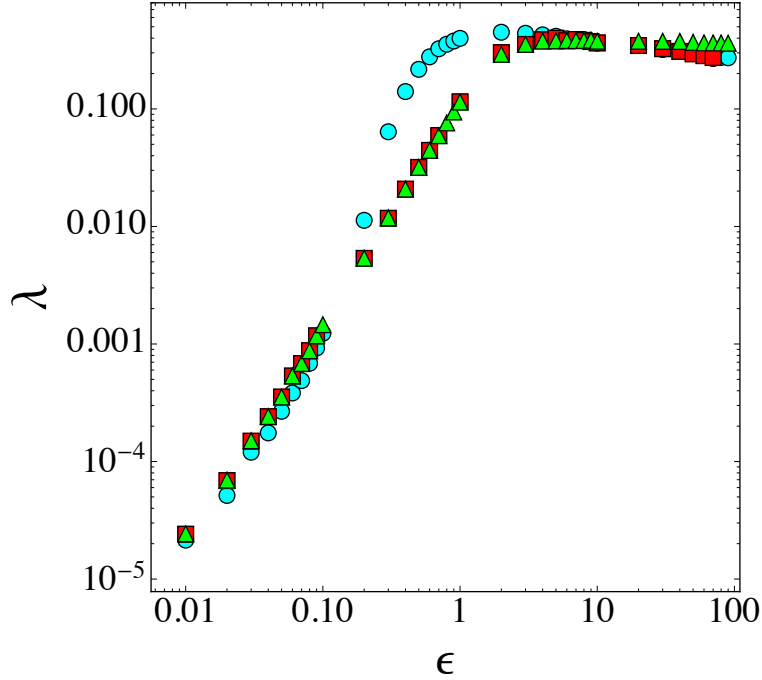


FIG. 10. Comparison between the two Geometric Lyapunov Exponents  $\lambda_{ge}$  (red squares),  $\lambda_{Ge}$  (green triangles) and the standard numerical computation of  $\lambda_1$  (cyan circles) vs energy density  $\epsilon$  for a system of  $N = 150$ . Here  $\eta = E$ .

The comparison among the outcomes  $\lambda_{g_e}(\epsilon)$ ,  $\lambda_{G_e}(\epsilon)$  of the "statistical" formula (53), and the standard computation of  $\lambda_1(\epsilon)$  are displayed in Figure 10. By standard computation of  $\lambda_1(\epsilon)$  we mean computing the average rate of the exponential growth of the norm of the tangent vector in Eq.(48) as per Eq.(45). The discrepancy, observed approximately for  $\epsilon$  in the interval between 0.2 and 2, has been given an explanation in Ref.[13] where it has been shown that the numerical distribution of the Ricci curvature of  $M \times \mathbb{R}^2$  actually displays a non-vanishing skewness with an excess of negative values with respect to a Gaussian distribution. This information is lost in the effective scalar model for the JLC equation above recalled. An *ad hoc* displacement of  $\langle k_R \rangle$  to empirically account for the excess of negative values of  $K_R$  allowed to exactly retrieve the pattern of  $\lambda_1(\epsilon)$  by means of the scalar effective model. A-priori the use of  $(M \times \mathbb{R}, G_e)$  could have fixed the problem more naturally but, disappointedly, this has not been the case thus calling for an improvement of the effective scalar model, possibly taking into account higher order moments of the Ricci curvature distribution. Finally, it is worth to mention that the potential function of the Hamiltonian (46) has a large number of critical points  $q_c$ , that is such that  $\nabla V(q)|_{q=q_c} = 0$  [11]; near each critical point, in Morse chart one has  $V(q) = V(q_c) - \sum_{i=1}^k q_i^2 + \sum_{i=k+1}^N q_i^2$  where  $k$  is the Morse index of a given critical point. Now, the neighborhoods of critical points are enhancers of chaos because using the expression for  $V(q)$  in Morse chart together with  $\nabla V(q_c) = 0$ , both equations (28) and (41) diagonalize with  $k$  unstable components in proximity of a critical point of index  $k$ . Morse theory relates critical points of a suitable real valued function (here the potential function) with topological properties of its levels sets, here of equipotential manifolds in configuration space. In other words, the 1D  $XY$  model highlights the necessity of taking into account also some topological property of the mechanical manifolds in order to improve the effective scalar model for the JLC equation.

## VII. DISCUSSION

Summarizing, the geometrization of Hamiltonian dynamics within the framework of the configuration space-time equipped with an Eisenhart metric,  $(M \times \mathbb{R}, G_e)$ , provides a correct distinction of regular and chaotic motions and it is in qualitative and quantitative agreement with the two other geometrization frameworks reported above. As already remarked, the advantage of this framework could be that of an intermediate level of complexity/richness of

its geometry with respect to  $(M_E, g_J)$  and  $(M \times \mathbb{R}^2, g_e)$  which could be useful in performing more elaborated investigations about the relation between geometry and chaos.

Let us conclude with an outlook at a prospective extension to generic dynamical systems of the geometric description of chaos in systems of differential equations

$$\dot{x}^i = f^i(x^1, \dots, x^N) = f^i(\mathbf{x}) \quad (55)$$

that is, also in the case of dissipative systems. By differentiation with respect to time of Eq.(55) we get a new system of equations

$$\ddot{x}^i = \sum_{j=1}^N \frac{\partial f^i(\mathbf{x})}{\partial x^j} \dot{x}^j = \sum_{j=1}^N \frac{\partial f^i(\mathbf{x})}{\partial x^j} f^j(\mathbf{x}) \quad (56)$$

that can be derived from the Lagrangian function

$$L(\mathbf{x}, \dot{\mathbf{x}}) = \sum_{i=1}^N [\dot{x}^i - f^i(\mathbf{x})]^2 \quad (57)$$

and the usual Lagrange equations. To this Lagrangian  $L(\mathbf{x}, \dot{\mathbf{x}})$  one associates a metric function homogeneous of degree one in the velocities

$$\Lambda(x^a, \dot{x}^a) = L(x^i, \dot{x}^i / \dot{x}^0) \dot{x}^0, \quad a = 0, 1, \dots, N; \quad i = 1, \dots, N \quad (58)$$

involving an extra velocity  $\dot{x}^0$ ; through this metric function a metric tensor expressed as

$$g_{ab}(\mathbf{x}, \dot{\mathbf{x}}) = \frac{1}{2} \frac{\partial^2 \Lambda^2}{\partial \dot{x}^a \partial \dot{x}^b} \quad (59)$$

provides the tangent bundle of the configuration space of the system (55) with a Finslerian structure. The geodesics of this space, minimizing the functional  $\int_{\tau_0}^{\tau_1} \Lambda(x^a, \dot{x}^a) d\tau$ , are given by [10, 24]

$$\frac{d^2 x^a}{ds^2} + \gamma_{bc}^a(\mathbf{x}, \dot{\mathbf{x}}) \frac{dx^b}{ds} \frac{dx^c}{ds} = 0 \quad (60)$$

where  $\gamma_{bc}^a(\mathbf{x}, \dot{\mathbf{x}})$  are the connection coefficients derived from the velocity dependent metric  $g_{ab}(\mathbf{x}, \dot{\mathbf{x}})$ , and coincide with the solutions of Eqs.(56). Then a geodesic deviation equation is defined also on Finsler manifolds and relates stability/instability of the geodesics with the curvature properties of the space [10]. This approach certainly deserves to be investigated to tackle chaotic dynamics of dissipative systems with the same methodological approach successfully applied to Hamiltonian systems.

## Acknowledgments

M.P. participated in this work within the framework of the project MOLINT which has received funding from the Excellence Initiative of Aix-Marseille University - A\*Midex, a French “Investissements d’Avenir” programme.

## APPENDIX A

### A remark about numerical integrations.

In order to faithfully represent the true trajectories of a Hamiltonian flow by means of numerical pseudo-trajectories one has to resort to symplectic algorithms. Symplectic algorithms compute the time evolution of the coordinates, that is  $\{p_i(t), q_i(t)\} \rightarrow \{p_i(t + \Delta t), q_i(t + \Delta t)\}$ , by performing a canonical transformation at each time step [25], therefore all the Poincaré invariants in phase space are conserved, in particular energy conservation and phase space volumes conservation (Liouville theorem) are fulfilled. Energy fluctuations  $\Delta E/E$  can be made arbitrarily small by reducing the integration time step. Any other kind of integration scheme, no matter if of high order, would not faithfully represent a Hamiltonian flow.

Symplectic algorithms are mappings producing pseudo orbits in phase space which, after Moser’s interpolation theorem [26, 27], are homeomorphic to true phase space trajectories via an homeomorphism which can be made arbitrarily close to the identity according to the value of  $\Delta t$ .

The simplest one is the leap-frog scheme which, for Hamiltonians of the form

$$H(\mathbf{p}, \mathbf{q}) = \sum_{i=1}^N \frac{p_i^2}{2} + V(\mathbf{q}) \quad (61)$$

reads as

$$\begin{aligned} q_i(t + \Delta t) &= q_i(t) + \Delta t \, p_i(t) \\ p_i(t + \Delta t) &= p_i(t) - \Delta t \nabla_i V[\mathbf{q}(t + \Delta t)] \quad . \end{aligned} \quad (62)$$

The precision of this integration scheme is considerably improved by resorting to a second order bilateral symplectic algorithm [23] which takes into account the exchangeability of the

$\{p_i(t)\}$  and  $\{q_i(t)\}$  under a suitable canonical transformation, it explicitly reads as

$$\begin{aligned}
(\mathbf{q}^{(0)}, \mathbf{p}^{(0)}) &= [\mathbf{q}(t), \mathbf{p}(t)] \\
q_i^{(1)} &= q_i(t) \\
p_i^{(1)} &= p_i(t) - \frac{1}{2} \Delta t \nabla_i V [\mathbf{q}^{(1)}] \\
q_i^{(2)} &= q_i^{(1)} + \Delta t p_i^{(1)} \\
p_i^{(2)} &= p_i^{(1)} - \frac{1}{2} \Delta t \nabla_i V [\mathbf{q}^{(2)}] \\
p_i^{(3)} &= p_i^{(2)} \\
q_i^{(3)} &= q_i^{(2)} + \frac{1}{2} \Delta t p_i^{(3)} \\
p_i^{(4)} &= p_i^{(3)} - \Delta t \nabla_i V [\mathbf{q}^{(3)}] \\
q_i^{(4)} &= q_i^{(3)} + \Delta t p_i^{(3)} \\
[\mathbf{q}(t + 2\Delta t), \mathbf{p}(t + 2\Delta t)] &= (\mathbf{q}^{(4)}, \mathbf{p}^{(4)}) .
\end{aligned} \tag{63}$$

For what concerns all the versions of the JLC equations, independently of the metric used, these are linear differential equations for the components of the geodesic separation vector, therefore any standard integration scheme is appropriate, e.g. like Runge-Kutta or predictor-corrector algorithms. Moreover, the JLC equations on the manifolds  $(M_E, g_J)$  and  $(M \times \mathbb{R}, G_e)$  contain both first and second order derivatives of their solutions preventing a treatment with symplectic integrators for these equations.

## APPENDIX B

The standard *operational* way to detect chaos and to quantify its strength is through Lyapunov characteristic exponents. A trajectory is said to be *chaotic* if its (largest) Lyapunov exponent  $\lambda_1$  is *positive*. It is customary to say that  $\lambda_1$  is an asymptotic quantity because its mathematical definition relies on Oseledec's multiplicative theorem [28]. Let us quickly recall why.

For a generic flow  $\varphi^t : M \rightarrow M$  on a manifold  $M$ , given an invariant measure,  $\mu$ , and denoting by  $d\varphi_x^t : T_x M \rightarrow T_{(\varphi^t x)} M$  its tangent dynamics, Oseledec's theorem ensures that  $\forall x \in M_1, \forall e \in T_x M$  ( $e \neq 0$ ), with  $M_1 \subset M$  and such that  $\mu(M_1) = 1$ , the quantity

$$\lambda(x, e) = \lim_{t \rightarrow \infty} \frac{1}{t} \ln \|d\varphi_x^t(e)\| , \tag{64}$$



which is independent of the metric of  $M$ , exists and is finite. More explicitly, let  $J(x)$  be the Jacobian matrix of the Hamiltonian flow  $\varphi^t$  at the point  $x = (p_1, \dots, p_N, q_1, \dots, q_N)$ . Denoting by  $\xi$  the variation vector, the tangent dynamics  $d\varphi^t$  is described by

$$\frac{d\xi_i}{dt} = J_{ik}(x(t))\xi_k .$$

A-priori, the largest positive eigenvector of the Jacobian matrix could give the local value of  $\lambda_1$ , however this possibility is ruled out by the fact that  $J : T_x M \rightarrow T_{(\varphi^t x)} M$  is not an endomorphism of a vector space. In other words, we do not know how the reference frames change going from  $T_x M$  to  $T_{(\varphi^t x)} M$  unless a connection on  $M$  is given. Thus we have to construct an endomorphism of, say,  $T_x M$ . This proceeds as follows. Take a vector  $\xi_x \in T_x M$  and its transformed  $\xi_{(\varphi^t x)} \in T_{(\varphi^t x)} M$ ; notice that

$$\langle \xi_{(\varphi^t x)}, J \xi_x \rangle = \langle J^* \xi_{(\varphi^t x)}, \xi_x \rangle$$

and that the product appearing at the left-hand side belongs to  $T_{(\varphi^t x)} M$ , while the product of the right-hand side necessarily belongs to  $T_x M$ , i.e.,  $J^* \xi_{(\varphi^t x)} \in T_x M$ , and in general  $\|\xi_{(\varphi^t x)}\| \neq \|\xi_x\|$ , whence  $J^* \neq J^{-1}$ . Therefore  $J$  maps the tangent vectors forward in time, while  $J^*$  maps these vectors backward in time but not retracing the forward evolution of  $\xi(t)$ . Having defined  $G = \prod_{i=1}^n J_i(\varphi^{i-1} x)$ , Oseledeč's theorem states that the limiting matrix

$$\Lambda_x = \lim_{n \rightarrow \infty} (G^* G)^{1/2n}$$

exists and is finite, and thus for any  $n$  the product  $(\prod_{i=1}^n J_i^*)(\prod_{k=1}^n J_k)$  maps an arbitrary vector  $\xi_x^0 \in T_x M$  into a vector  $\xi_x^n \in T_x M$ , i.e., into the *same* tangent space  $T_x M$ . Thus an eigenvalue problem for  $\Lambda_x$  is well defined in the vector space  $T_x M$ .

Having derived the tangent dynamics equation (28) - which is used to compute  $\lambda_1$  for Hamiltonians of the form (64) - by means of the JLC equation for the Eisenhart metric on  $M \times \mathbb{R}^2$ , means having recognized its covariant nature. This means that the way the reference frames change going from  $T_x M$  to  $T_{(\varphi^t x)} M$  is automatically taken into account by the Levi-Civita connection of the manifold  $M \times \mathbb{R}^2$ . As a consequence, there is no longer any need to invoke the asymptotic property of  $\lambda_1$  which is also locally well defined and

meaningful.

- 
- [1] J. Guckenheimer and P. Holmes, *Nonlinear Oscillations, Dynamical Systems and Bifurcations of Vector Fields*, (Springer-Verlag, Berlin, 1983).
  - [2] S. Wiggins, *Global Bifurcations and Chaos*, AMS Series No. 73 (Springer, New York, 1988).
  - [3] A. J. Lichtenberg and M. A. Lieberman, *Regular and Chaotic Dynamics*, (Springer-Verlag, Berlin, 1992).
  - [4] H. Poincaré, *Les Méthodes Nouvelles de la Mécanique Celeste*, (Blanchard, Paris, 1987).
  - [5] H. Hénon and C. Heiles, *The applicability of the third integral of motion: Some numerical experiments*, Astron. J. **69**, 73 (1964).
  - [6] H. Poincaré, *Les Méthodes Nouvelles de la Mécanique Celeste*, (Blanchard, Paris, 1987), vol. 3, p.389.
  - [7] D. V. Anosov, *Geodesic flows on closed Riemannian manifolds of negative curvature*, Proc. Steklov Math. Inst. **90**, 1-235 (1967).
  - [8] N. S. Krylov, *Works on the Foundations of Statistical Physics*, (Princeton University Press, Princeton, 1979).
  - [9] The natural and elegant geometric setting of Hamiltonian dynamics is provided by symplectic geometry. This geometrical framework is very powerful to study, for example, symmetries. However, symplectic manifolds are not endowed with a metric, and without a metric we do not know how to measure the distance between two nearby phase space trajectories and thus to study their stability/instability through the time evolution of such a distance.
  - [10] M. Pettini, *Geometrical hints for a nonperturbative approach to Hamiltonian dynamics*, Phys. Rev. E **47**, 828 (1993).
  - [11] M. Pettini, *Geometry and Topology in Hamiltonian Dynamics and Statistical Mechanics*, IAM Series n.33, (Springer, New York, 2007).
  - [12] The original formulation of the Poincaré-Birkhoff theorem holds for two dimensional systems, however several generalizations at arbitrary dimension are available, see for example: A. Fonda and A. J. Urenã, *A higher dimensional Poincaré-Birkhoff theorem for Hamiltonian flows*, Ann. Inst. H. Poincaré Anal. Non Linéaire **34**, 679 (2017).
  - [13] L. Casetti, C. Clementi, and M. Pettini, *Riemannian theory of Hamiltonian chaos and Lya-*

- Lyapunov exponents*, Phys. Rev. E **54**, 5969 (1996).
- [14] L. P. Eisenhart, *Dynamical trajectories and geodesics*, Ann. Math. **30**, 591 (1929).
  - [15] A. Lichnerowicz, *Théories Relativistes de la Gravitation et de l'Electromagnetisme*, (Masson, Paris, 1955).
  - [16] E. Cuervo-Reyes and R. Movassagh, *Non-affine geometrization can lead to non-physical instabilities*, J. Phys. A: Math. and Theor. **48**, 075101 (2015).
  - [17] M. Pettini and R. Valdettaro, *On the Riemannian description of chaotic instability in Hamiltonian dynamics*, CHAOS **5**, 646 (1995).
  - [18] M. Cerruti-Sola and M. Pettini, *Geometric description of chaos in two-degrees-of-freedom hamiltonian systems*, Phys. Rev. E **53**, 179 (1996).
  - [19] M. Cerruti-Sola, R. Franzosi, and M. Pettini, *Lyapunov exponents from geodesic spread in configuration space*, Phys. Rev. E **56**, 4872 (1997).
  - [20] L. Di Cairano, M. Gori, and M. Pettini, *Coherent Riemannian-geometric description of Hamiltonian order and chaos with Jacobi metric*, Chaos **29**, 123134 (2019);
  - [21] R. Livi, M. Pettini, Stefano Ruffo, and Angelo Vulpiani, *Chaotic Behavior in Nonlinear Hamiltonian Systems and Equilibrium Statistical Mechanics*, J. Stat. Phys. **48**, 539 (1987).
  - [22] C. Clementi and M. Pettini, *A geometric interpretation of integrable motions*, Cel. Mech. & Dyn. Astron. **84**, 263 (2002).
  - [23] L. Casetti, *Efficient symplectic algorithms for numerical simulations of Hamiltonian flows*, Physica Scripta **51**, 29 (1995).
  - [24] H. Rund, *The Differential Geometry of Finsler Spaces*, (Springer-Verlag, Berlin, 1959).
  - [25] The generating function of the canonical transformation corresponding to the basic leap-frog algorithm can be found in: M. Pettini, and M. Landolfi, *Relaxation properties and ergodicity breaking in nonlinear hamiltonian dynamics*, Phys. Rev. A **41**, 768 (1990).
  - [26] J.K. Moser, *Lectures on Hamiltonian systems*, Mem. Am. Math. Soc. **81**, 1 - 60 (1968).
  - [27] G. Benettin, and A. Giorgilli, *On the Hamiltonian interpolation of near-to-the identity symplectic mappings with application to symplectic integration algorithms*, J. Stat. Phys. **73**, 1117 - 1143 (1994).
  - [28] V. I. Oseledec, *A multiplicative ergodic theorem. Characteristic Lyapunov exponents of dynamical systems*, Trans. Moscow Math. Soc. **19**, 197 (1969).